

Development of multiple tidal tails around globular clusters and dwarf satellite galaxies

Shunsuke Hozumi^{1*} and Andreas Burkert^{2,3†}

¹*Faculty of Education, Shiga University, 2-5-1 Hiratsu, Otsu, Shiga 520-0862, Japan*

²*Universitätssternwarte der Ludwig-Maximilians Universität, Scheinerstr. 1, D-81679 München, Germany*

³*Max-Planck-Institut für Extraterrestrische Physik, Giessenbachstr. 1, D-85748 Garching, Germany*

Accepted 2014 October 29; Received 2014 September 7; in original form 2014 August 11

ABSTRACT

The formation and evolution of tidal tails like those observed around some globular clusters and dwarf satellite galaxies is examined with an N -body simulation. In particular, we analyse in detail the evolving tidal features of a one-component satellite that is moving on a highly eccentric orbit in the external field of a host galaxy potential like our own. The results show that every time the satellite approaches apogalacticon, a fresh pair of tidal tails becomes notably prominent, and that eventually, the satellite possesses multiple tidal tails via repeating apocentre passages. Accordingly, the number of observed tidal arms can be used as a tracer of the number of orbital periods that such a system has completed around the centre of its host galaxy. By identifying the arm particles included in each of the first three consecutively formed pairs of tidal tails, we find that each pair of tidal tails is practically identical to one another regarding the energy and angular momentum distributions. In addition, we demonstrate that the density profiles of these three pairs of tidal tails at their first apogalacticons after formation agree well with one another. It therefore follows that the multiplicity in tidal features originates from the repeated episode of tidal arm formation in the course of the precessing motion of a satellite.

Key words: methods: numerical – globular clusters: general – galaxies: dwarf – galaxies: kinematics and dynamics.

1 INTRODUCTION

Recently, the observational evidence for tidal tails around globular clusters (GCs) has been growing since Grillmair et al. (1995) pointed out wing-like structures in the surface density profiles of GCs as a signature of tidal tails. Subsequent observations have confirmed and reinforced Grillmair et al.’s (1995) findings (amongst many others, Lehmann & Scholz 1997; Leon, Meylan & Combes 2000; Testa et al. 2000; Siegel et al. 2001; Lee et al. 2003; Balbinot et al. 2011; Sollima et al. 2011), providing further pieces of evidence that support the existence of tidal tails associated with GCs. Above all, Palomar 5 is well known for its two long and massive tidal tails that extend to the opposite directions from the main body (Odenkirchen et al. 2001, 2002, 2003), and NGC 5466 is also known to have extended giant tails (Belokurov et al. 2006; Grillmair & Johnson 2006). These two GCs are representative examples of ongoing tidally disrupting stellar systems in the Milky Way.

Indications of tidal features have also been observed in some dwarf galaxies. For instance, among Milky Way satellites, a tidal extension was found in Ursa Minor (Martínez-Delgado et al. 2001a), and an excess distribution of stars induced by tidal interactions was detected around Carina (Muñoz et al. 2006) and Leo I (Sohn et al. 2007). As another example, the surface brightness around Fornax was shown to depend on the direction of measurement (Coleman et al. 2005), which is reminiscent of tidal distortion. Even outside the Milky Way, strong tidal features have been discovered e.g. around the Andromeda satellite, NGC 205 (Howley et al. 2008; Saviane, Monaco & Hallas 2010) or around a dwarf galaxy in the Hydra I galaxy cluster that belongs to the Local Volume (Koch et al. 2012; Rich et al. 2012). Furthermore, a dwarf galaxy in the act of tidal disruption has been reported in the halo of NGC 4449 which is also a dwarf galaxy in the nearby Universe (Martínez-Delgado et al. 2012).

As described above, tidal tails are common features of satellite systems moving around a host galaxy. In such a situation, the force field of the host in which a satellite is orbiting will lead to the formation of a variety of tidal tails around the satellite. Consequently, we can estimate the dis-

* E-mail: hozumi@edu.shiga-u.ac.jp

† Max Planck Fellow.

tribution of the gravitational potential of the host galaxy from the morphology of the tidal tails (e.g. Binney 2008). Since Galactic GCs are, on average, distributed much closer to the centre of our Galaxy than satellite dwarf galaxies, the tidal tails of GCs can give an indication of the inner mass profile of our Galaxy, while those of satellite dwarf galaxies can be used as a probe for the outer mass distribution. In addition, if the morphology of tidal tails could help to trace the orbit of a GC or a dwarf galaxy, we might be able to obtain an assembly history of satellite systems through which a galaxy is built up and eventually becomes a large and massive grown-up. Thus, through the tidal tails of satellite systems, we could verify observationally the hierarchical structure formation scenario (e.g. Boylan-Kolchin et al. 2010).

From the viewpoints mentioned above, many numerical simulations have been carried out so far regarding the tidal interactions between a satellite system and its host galaxy (Piatek & Pryor 1995; Grillmair 1998; Mateo, Olszewski & Morrison 1998; Martínez-Delgado et al. 2001a,b, 2004; Dehnen et al. 2004; Capuzzo Dolcetta, Di Matteo & Miocchi 2005; Choi, Weingerg & Katz 2007; Montuori et al. 2007; Klimentowski et al. 2009; Peñarrubia et al. 2009; Küpper, Lane & Heggie 2012; Lokas, Gajda & Kazantzidis 2013). Some studies have focused on the connection between the orientation of tidal tails and the satellite orbit in order to examine whether the orbital path of a satellite can be determined from the observed morphology of its tidal tails (Capuzzo Dolcetta et al. 2005; Montuori et al. 2007; Klimentowski et al. 2009; Lokas et al. 2013). Unfortunately, the orientation of the tails is not a direct indicator of the orbital path, because it depends on the orbital phase: the tidal tails start to develop with the orientation almost parallel to the orbital path near the pericentre and the orientation changes gradually over time to become perpendicular near the apocentre if the orbit is relatively eccentric. However, as stated by Montuori et al. (2007), the tails located quite far from the GC centre are good tracers of the GC path. This is because the tidal tails continue to extend along both sides of the cluster path with time, once the cluster has passed the first apocentre after the tails were extracted near the pericentre.

Although considerable attention has been paid to the direction of tidal tails around satellite systems, there are no sufficient descriptions of the complicated features of tidal tails that are forming while a satellite system is moving on an eccentric orbit. In fact, intricate features like multiple tidal arms can be seen in the simulations of Dehnen et al. (2004), Capuzzo Dolcetta et al. (2005), and Montuori et al. (2007). Montuori et al. (2007) noted the peculiar morphology of multiple arms when the cluster was approaching the apocentre. They explained the difference in the direction of tidal arms at the pericentre and apocentre based on the direction and strength of the Coriolis acceleration at both positions. Indeed, their explanation describes how the direction of a given pair of tidal arms changes as its main body moves on an eccentric orbit. However, how the multiplicity is formed during the orbital motion has never been elucidated exactly.

In this paper, we aim at disclosing the formation mechanism of multiple tidal tails around a satellite using an N -body simulation. In doing so, we pay attention only to collisionless systems and we will ignore the internal evolution

caused by two-body relaxation in the case of collisional systems like GCs. However, as the two-body relaxation time-scale is typically long compared to an orbital period, we expect collisional effects in GCs to be negligible, especially in the outer regions where the tidal tails develop. In order to keep the analyses simple, we also neglect the fact that dwarf spheroidal galaxies are in effect two-component systems, consisting of a stellar inner spheroid embedded in a surrounding dark halo component. This is justified by the fact that dwarf spheroidals are characterized by large mass-to-light ratios (Mateo 1998; Gilmore et al. 2007), indicating that the self-gravity of the stellar component is negligible. Dwarf spheroidals therefore to a good approximation can be treated as a one-component system with the stars tracing the inner part of the tidally distorted dark matter component.

In Section 2, we describe our model of a satellite and its host galaxy, and the N -body simulation method, together with the initial set-up of the simulation. For convenience, we will call our satellite a dwarf galaxy and we will adopt typical physical parameters that apply to such systems. Note, however, that all parameters can be rescaled to correspond to systems with smaller masses so as to be adjusted more suitably for GCs. Results are presented in Section 3. In Section 4, we discuss the formation mechanism of the multiple tidal tails and the detectability of such tidal tails. Finally, conclusions are given in Section 5.

2 MODELS AND METHOD

We follow the dynamical evolution of a satellite that is tidally interacting with its host galaxy. In particular, our objective is to understand the mechanism by which multiple tidal tails develop in the course of the orbital motion of the satellite. For this purpose, we choose a single typical set-up that will cause the multiplicity in tidal tails, and analyse its formation process in detail.

The host galaxy is represented as an external potential that consists of an infinitely extended isothermal sphere. Its potential, Φ , is written as

$$\Phi(r) = v_c^2 \ln(r/r_0), \quad (1)$$

where r is the radial distance from the centre of the host galaxy, r_0 is a reference radius which, for conventional reasons, ensures negative values of the potential over a practical range of radii, and v_c is a constant circular velocity. This host galaxy corresponds to an extremely simplified model of a dark matter halo that leads to the flat rotation curve often observed in disc galaxies (Sofue & Rubin 2001). In this model, a disc component is not included, so that we do not take into account the effects of disc shocking that would be suffered by a satellite when it penetrates the disc, and those of likely precession of the satellite orbit that would arise from the resulting asymmetric gravitational field. Since the pericentre distance of our dwarf galaxy model is 20 kpc as described below, these effects could be negligibly small, which means that we could be allowed to neglect them. However, if our adopted parameters are rescaled to be adjusted to GCs, a disc component would be needed to evaluate these effects. Although the simulation is scale free, for better demonstra-

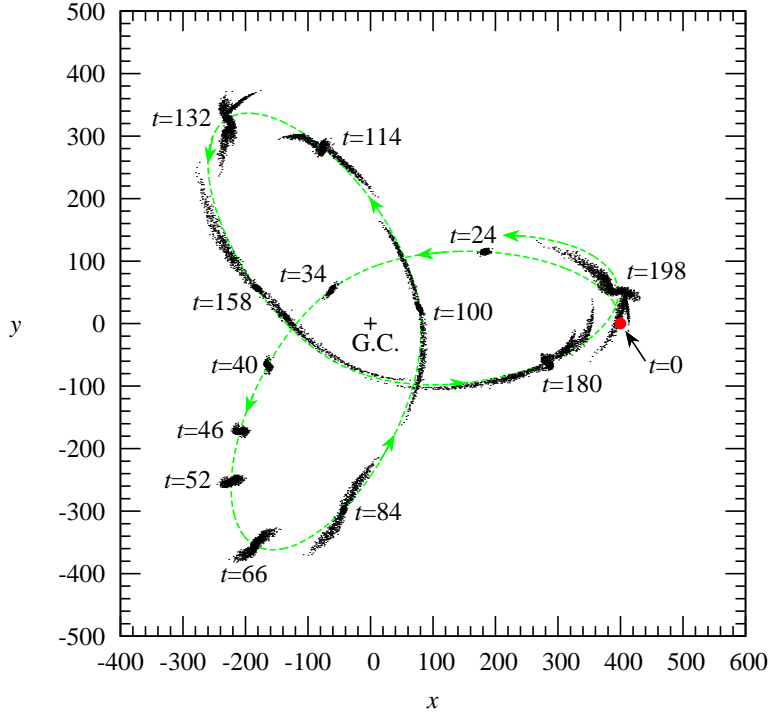


Figure 1. Time evolution of the dwarf satellite galaxy in the act of tidal interaction with its host galaxy from the beginning till $t = 198$. The particle distribution is seen in the orbital ($x - y$) plane. At times denoted by the labels, one-tenth of all particles at each position of the dwarf galaxy are randomly selected and displayed. The filled red circle at $(400, 0)$ stands for the initial position of the dwarf galaxy, and the + symbol represents the centre of the host galaxy. The dashed green line shows the orbital path of the dwarf galaxy that moves in the directions of the arrows. The dwarf galaxy is represented on real scales.

tion we adopt $r_0 = 125$ kpc and $v_c = 220$ km s $^{-1}$ to mimic a typical real Milky Way-type galaxy.

The satellite is modelled as a Plummer sphere (Plummer 1911) whose density, ρ_d , and potential, Φ_d , are, respectively, given by

$$\rho_d(r') = \frac{3M}{4\pi a^3} [1 + (r'/a)^2]^{-5/2}, \quad (2)$$

and

$$\Phi_d(r') = -\frac{GM}{a} [1 + (r'/a)^2]^{-1/2}, \quad (3)$$

where G is the gravitational constant, M and a are the mass and scale length of the satellite, respectively, and r' stands for the radial distance from its centre. We realize this model with $N = 50\,000$ particles of equal mass by truncating it at $r' = 5a$. As a result, its total mass amounts to 94.3 per cent of the corresponding perfect Plummer sphere. For the satellite constructed here, however, M is assigned to this finite model. We use $M = 10^7 M_\odot$ and $a = 0.25$ kpc as typical values, corresponding to a dwarf satellite galaxy. This satellite galaxy is put into an orbit with an eccentricity of two-thirds, the value of which is suitable for the formation of multiple tidal arms (Dehnen et al. 2004; Montuori et al. 2007), as well as typical for most dwarf galaxies formed in cosmological simulations (Diemand, Kuhlen & Madau 2007). Here, the eccentricity, ϵ , is defined as

$$\epsilon = \frac{r_a - r_p}{r_a + r_p}, \quad (4)$$

where r_a and r_p are the apo- and peri-galactic distances, respectively. We set r_a to be 100 kpc and r_p to be 20 kpc,

and commence a simulation by placing the dwarf galaxy at apogalacticon. From the beginning, the full host potential was imposed on the dwarf galaxy. This set-up procedure would not harm the entire dynamics of the dwarf galaxy, since the crossing time, t_{cr} , of the dwarf galaxy, as estimated at the half-mass radius, r'_h , is approximately one-twentieth of the orbital time-scale, when t_{cr} is calculated as $t_{cr} = r'_h/\sigma_0$, where σ_0 is the one-component velocity dispersion at r'_h .

The simulation was carried out with a hierarchical tree algorithm (Barnes & Hut 1986). Forces were computed with an opening angle of 0.5 and a gravitational softening of $0.068a$, including terms up to quadrupole order in the multipole expansions. The equations of motion were integrated in Cartesian coordinates with a time-centred leap-frog algorithm (e.g. Press et al. 1986). Results are presented in the system of units such that $G = M = a = 1$. Thus, when scaled to physical values, unit time and velocity are 1.86×10^7 yr and 13.1 km s $^{-1}$, respectively. The simulation was continued until time $t = 500$ with a constant time step of 0.05, which guaranteed that the total energy of the system was conserved to better than 1.67×10^{-4} .

3 RESULTS

Fig. 1 shows the time evolution of the dwarf galaxy that is suffering tidal forces from its host galaxy. This figure reveals the formation process of tidal tails, with the dwarf galaxy being heavily deformed over time. In particular, we can see that tidal tails became progressively very intricate. Since

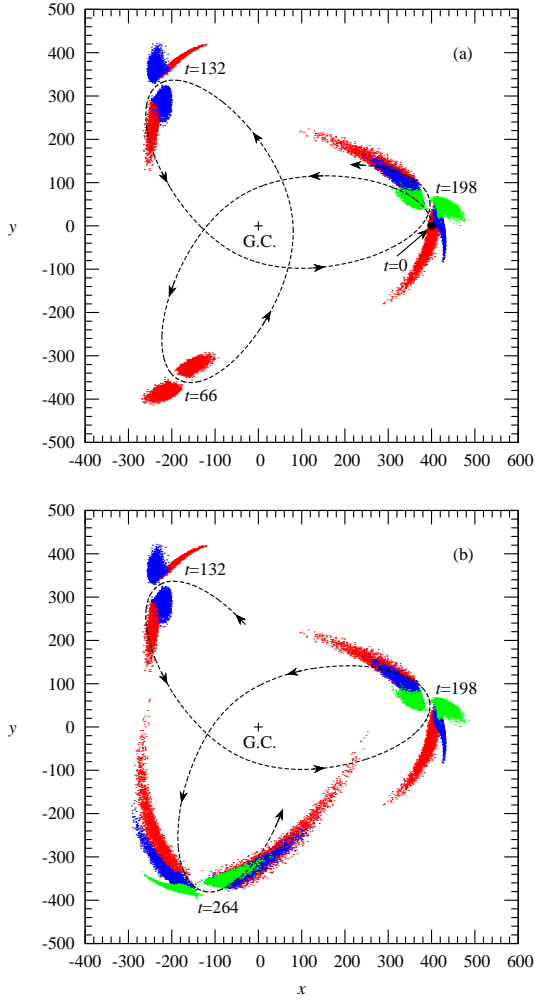


Figure 2. Forming and evolving phases of tidal tails seen in the orbital plane from $t = 0$ to 198 (a), and from $t = 132$ to 264 (b). Only the particles included in each of the first three consecutively formed pairs of tidal arms are shown without depicting the main body of the dwarf galaxy. In reality, the fourth pair of tidal arms is formed at $t = 264$, which is omitted in this plot. The red, blue, and green dots represent the particles of the tidal arms formed first, secondly, and thirdly, respectively, from the beginning of the simulation. The dashed lines trace the orbit of the centre of the dwarf galaxy, with the arrows indicating the moving directions of the orbit. The filled circle at (400, 0) in (a) denotes the initial position of the dwarf galaxy. The + symbols indicate the centre of the host galaxy. Note that the tidal tails are magnified twice as large as in reality for convenience in illustration.

the principal aim of our study is to unravel how these complicated tidal structures illustrated in Fig. 1 are formed, it is useful to decompose the tidal arms in chronological order. In order to distinguish the particles contained in the first formed tidal tails from the main body, we select particles which are both marginally bound to and unbound from the main body at the first apogalacticon (at $t \sim 66$), and then, from these particles, we determine the particles that are unbound from the main body afterwards all the way to the end of the simulation ($t = 500$). Eventually, we have identified the first formed tidal tails. Then, repeating this procedure at the subsequent two apogalacticons (at $t \sim 132$

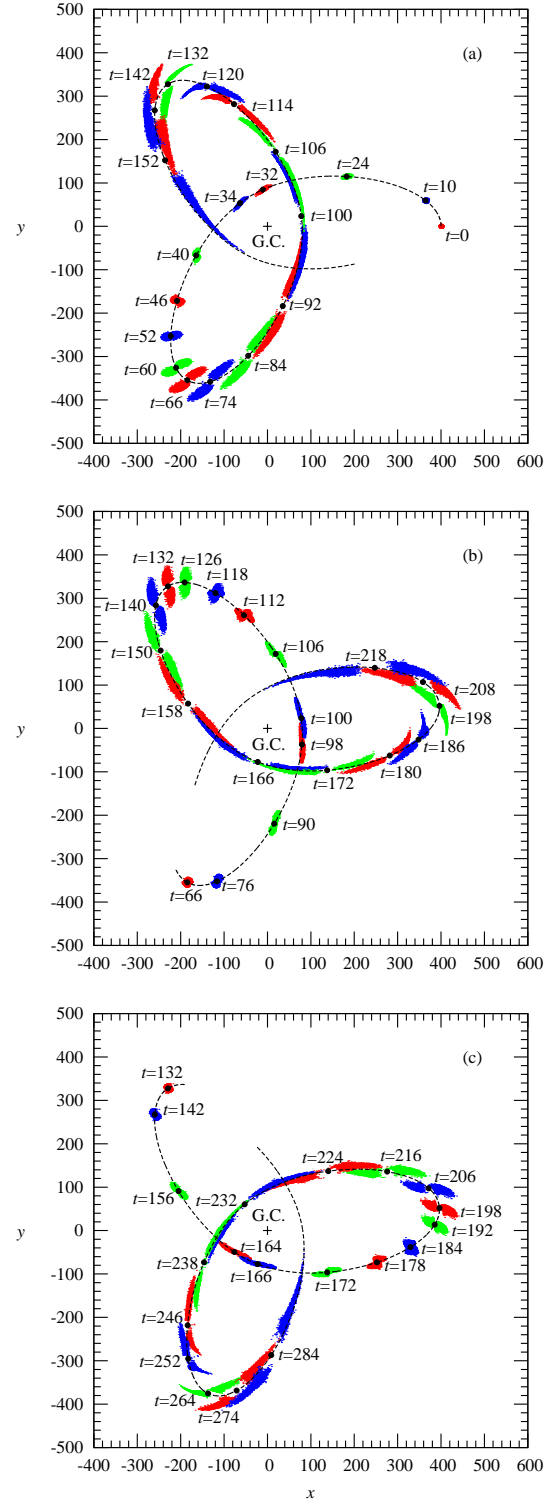


Figure 3. Time evolution of the tidal arms formed first (a), secondly (b), and thirdly (c) seen in the orbital plane. Again, only the particles included in each pair of tidal arms are displayed. The filled circles denote the centre of the dwarf galaxy at times shown by the labels. In each panel, the starting time for plotting arms is very close to apogalacticon, and the subsequent plotting time intervals are the same for the three pairs of tidal arms. The three colours of red, blue, and green are repeatedly used in this order with time just for the purpose of facilitating visualization. The tidal tails are depicted on real scales unlike those in Fig. 2.

and ~ 198) while eliminating particles already confirmed as arm particles, we can single out the particles belonging to the secondly and thirdly formed tidal tails. Fig. 2 displays the forming and evolving phases of the three groups of tidal arms thus classified by virtue of the formation epoch, with the main body of the dwarf galaxy being masked. As found from this figure, the arm particles formed at each epoch can be separated into either leading-arm or trailing-arm particles on the basis of their positions relative to the main body when seen in the orbital plane.

We find from Fig. 2 that a pair of tidal arms is newly generated every time the dwarf galaxy completes a sequential move from one apogalacticon to another, and that the evolution of each pair of tidal arms looks very similar to one another. For example, the pair of tidal arms at $t = 66$ represented with red dots resembles the two pairs of those which appear at $t = 132$ with blue dots and at $t = 198$ with green dots. Likewise, the pair of the secondly formed tidal tails at $t = 198$ marked with blue dots has similar appearance to the pair of those at $t = 264$ with green dots.

Fig. 3 exhibits the time evolution of the first three pairs of tidal arms separately, again without depicting the main body. This figure clearly demonstrates that the formation and evolution of the secondly formed pair of tidal arms is one episode behind those of the first formed pair, and that this relation between the first and secondly formed pairs is basically repeated by the secondly and thirdly formed pairs concerning the formation and evolution of tidal arms. However, there are also some minor differences. The particles contained in the first pair are distributed rather compactly from the beginning to $t = 46$ somewhat after the first pericentre passage as compared to those in the second and third pairs which show expanded distributions from the time around apocentre passage ($t = 66$ for the second pair and $t = 132$ for the third pair) to the time somewhat after pericentre passage ($t = 112$ for the second pair and $t = 178$ for the third pair). This is because the particles in the second and third pairs have already suffered tidal effects once (the third pair) or twice (the second pair) in passing pericentre (see also Fig. 4). Nevertheless, except at the early formation phases, the appearance of the three pairs of tidal arms at each corresponding phase looks very similar to one another.

Fig. 4 shows the time evolution of the mean specific energy, $\langle E \rangle$, and that of the mean specific angular momentum, $\langle J \rangle$, each of which is calculated by averaging over all particles included in each leading or trailing arm of the first three consecutively formed tidal tails, along with the radial distance between the centres of the dwarf and host galaxies against time. To be precise, the specific energy is the total energy, and includes both potentials of the dwarf and host galaxies, while the specific angular momentum is its absolute value being calculated with respect to the centre of the host galaxy. From Fig. 4, we find that the dwarf galaxy suffers strong tidal forces within the potential of the host galaxy when it passes pericentre, which leads to the excitation of a pair of tidal tails, and that as a consequence, particles in trailing arms gain both energy and angular momentum, while those in leading arms lose both energy and angular momentum. Although all arm particles gain some energy and subsequently become unbound from the dwarf galaxy, the total energies of those leading-arm particles, which are moving slightly inside the orbital path of the dwarf galaxy

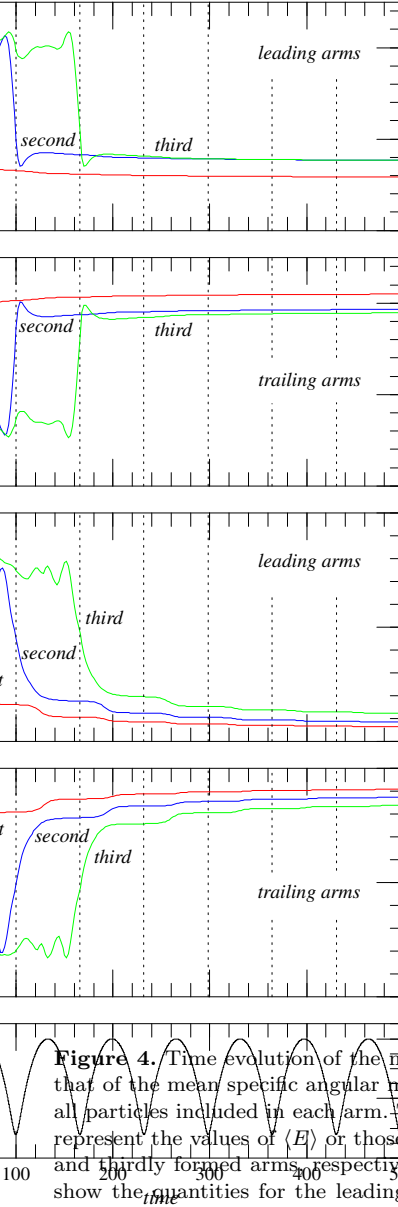


Figure 4. Time evolution of the mean specific energy, $\langle E \rangle$, and that of the mean specific angular momentum, $\langle J \rangle$, averaged over all particles included in each arm. The red, blue, and green lines represent the values of $\langle E \rangle$ or those of $\langle J \rangle$ for the first, secondly, and thirdly formed arms, respectively. The top and third panels show the quantities for the leading arms, while the second and fourth panels show those for the trailing arms. The vertical dotted lines denote the times of pericentre passage. The bottom panel indicates the radial distance between the centres of the dwarf and host galaxies as a function of time.

after being tidally extracted, decrease by an amount which is much larger than the gained energy owing to further energy loss that originates from the difference in the host galaxy potential between the particle positions before and after the tidal extraction. We provide estimations of the energy and angular momentum changes for the arm particles at the formation epoch in Appendix A. In addition, we notice from Fig. 4 that leading-arm (trailing-arm) particles periodically lose (gain) angular momentum by a tiny amount after they

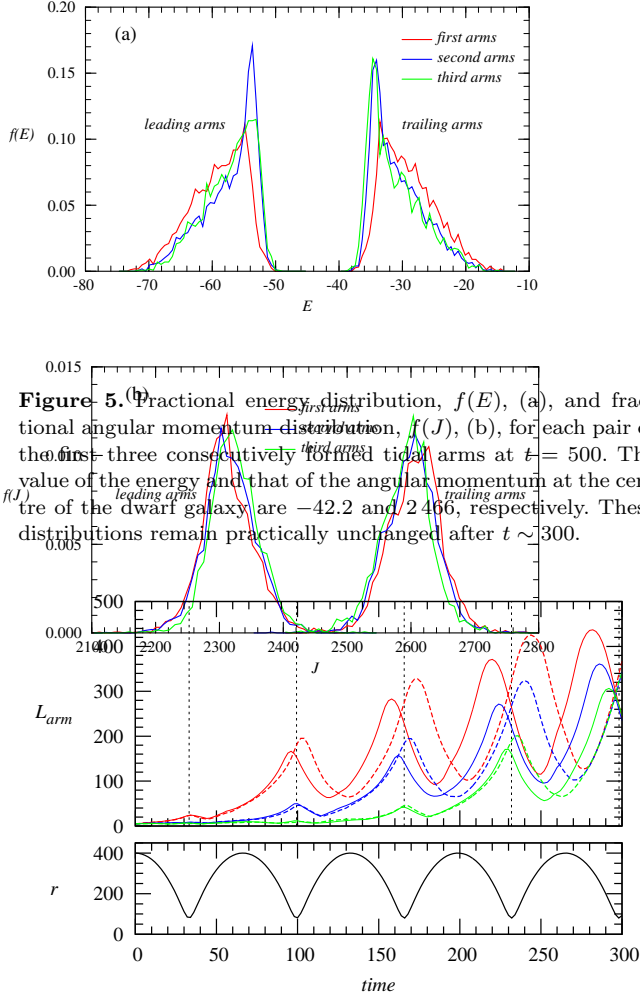


Figure 5. Fractional energy distribution, $f(E)$, (a), and fractional angular momentum distribution, $f(J)$, (b), for each pair of the first three consecutively formed tidal arms at $t = 500$. The value of the energy and that of the angular momentum at the centre of the dwarf galaxy are -42.2 and 2466 , respectively. These distributions remain practically unchanged after $t \sim 300$.

Figure 6. Time evolution of the lengths of leading (solid lines) and trailing (dashed lines) arms (upper panel), and time change in the radial distance between the centres of the dwarf and host galaxies (lower panel). The length of an arm is the distance between the nearest and farthest particles in the arm from the centre of the dwarf galaxy. The red, blue, and green lines represent the lengths of the first, secondly, and thirdly formed tidal arms, respectively. The vertical dotted lines indicate the times of pericentre passage.

escape from the dwarf galaxy and form tidal tails; a closer look at the late time evolution in the figure indicates that the subsequent changes in angular momentum of arm particles occur not near perigalacticon but near apogalacticon. This angular momentum change is caused by the gravitational force of the main satellite body that attracts the leading-arm particles backward and the trailing-arm particles for-

ward, and that the effect of the attractive force is largest at apogalacticon where the arm particles are closest to the satellite (see Fig. 6).

Figs 5(a) and 5(b) present, respectively, the fractional energy distribution, $f(E)$, and the fractional angular momentum distribution, $f(J)$, for each pair of the first three consecutively formed tidal arms at the end of the simulation ($t = 500$). As found from Fig. 4, the arm particles experience only a small amount of change in energy and angular momentum after they have escaped from the potential of the satellite, and so, the distributions of energy and angular momentum for the first three pairs of tidal tails can be regarded as approximately invariable if they are examined at times somewhat later than the formation of the third pair of tidal arms. Thus, Figs 5(a) and 5(b) indicate that the energy and angular momentum distributions of the three pairs of tidal arms are almost identical to one another. Particularly remarkable is the agreement in $f(J)$ for both leading and trailing arms among the three pairs of tidal arms.

Fig. 6 shows the time evolution of the lengths of leading and trailing arms for the first three consecutively formed tidal arms. Here, we define the length of an arm as the linear distance between the nearest and farthest particles in the arm from the centre of the dwarf galaxy. For each pair of tidal arms, the lengths of the leading and trailing arms become longer and longer as the dwarf galaxy moves from an apogalacticon to the next perigalacticon, and they become shorter and shorter as it moves from that perigalacticon to the next apogalacticon. The length of each arm as a whole shows a gradual increase over time, while this oscillatory behaviour in the arm length is repeated. The change in the length of tidal tails has often been mentioned qualitatively (e.g. Lokas et al. 2013). This figure demonstrates quantitatively what we have found from Fig. 3: the time change in the tidal arm lengths of the secondly formed pair is one episode behind that of the first formed pair, and this relation between the first and secondly formed pairs holds also between the secondly and thirdly formed pairs.

To illustrate that the three pairs of tidal tails have similar shapes and density distributions, we first rotate the positions of the arm particles projected on to the orbital plane in the secondly formed tails by the angle between the two apogalacticons at $t \sim 132$ and ~ 198 , and superpose the secondly formed tails on the first formed tails at the positions of the trailing and leading arms of the first formed tails at $t = 132$. Next, these processes are also applied to the secondly and thirdly formed tails, for which the rotation angle is the one between the two apogalacticons at $t \sim 198$ and ~ 264 , and the superposition is carried out again at the positions of those arms of the first formed tails at $t = 132$. In Fig. 7, we present such superpositions of the density contours of the first three consecutively formed tidal tails, when they are seen in the orbital plane. From the left-hand panels of Figs 7(a) and 7(b), we can see that at least, the outlines of the three trailing and leading arms are in fairly good agreement with one another. In addition, the density distributions of the first formed tidal tails do not deviate considerably from those of the secondly formed ones both for the trailing and leading arms, as illustrated in the middle panels of Figs 7(a) and 7(b). Likewise, the density distributions of the secondly formed tidal tails agree to some extent with those of the thirdly formed ones again both for the trailing

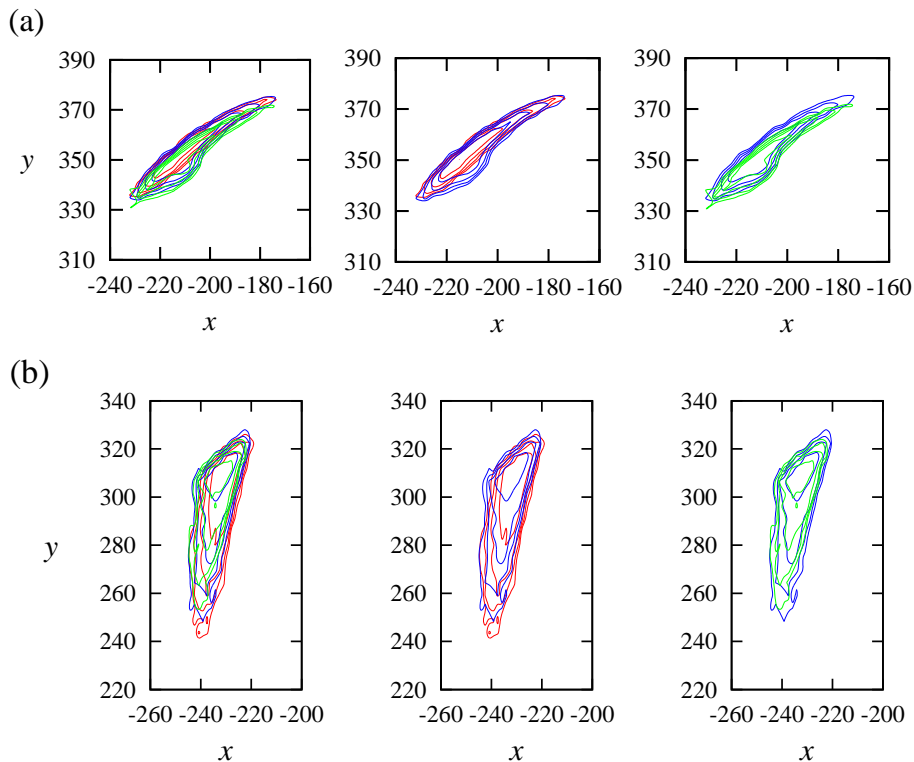


Figure 7. Superposition of the density contours projected on to the orbital plane of the first three consecutively formed tidal tails by rotating an angle between two specified apogalacticons for trailing arms (a) and leading arms (b). All three arms (left-hand panels), the first (at $t = 132$) and second (at $t = 198$) arms (middle panels), and the second (at $t = 198$) and third (at $t = 264$) arms (right-hand panels) are superposed at the positions of the first trailing and leading arms at $t = 132$. The density contours are drawn at the 80, 60, 40, and 20 per cent levels of the maximum density of each arm on logarithmic scales. The red, blue, and green contours denote the density contours of the first, second, and third arms, respectively.

and leading arms, as recognized from the right-hand panels of Figs 7(a) and 7(b).

In Fig. 8, we show the snapshots of the tidal arms at $t = 104$ and 170, somewhat after pericentre passage without depicting the main body of the dwarf galaxy. This figure indicates that at $t = 104$, the particles constituting the first pair of tidal arms are already farther away from the main body and distributed along either side of its orbital path. The situation is similar at $t = 170$ when both the first and second arms have disconnected from the main body. As a result, the region in the vicinity of the main body is always occupied by the particles that are forming a new pair of tidal arms. However, as the dwarf galaxy approaches apogalacticon, many of the constituent particles of the existing pair(s) come closer to the main body and the lengths of the arms shrink, as illustrated in Figs 2 and 6. In this way, the existing pair(s) and the newly formed pair of tidal arms are found together in the vicinity of the main body around apocentre passage, as is evident from the snapshots at $t = 132$ and 198 in Fig. 2. We also notice that each of the consecutively formed leading and trailing arms is smoothly connected in line near perigalacticon, which looks as if only a single pair of tidal arms were created.

As a side note, Fig. 9 presents the spherically averaged density profiles of the main body of the dwarf galaxy at the times around apogalacticon. We have confirmed that the main body itself is roughly spherical within $r' \sim 10$ until $t \sim 200$. As seen from this figure, the initial density profile is

deformed outside of $r \sim 2$, the radius of which is considered to be the tidal radius. Indeed, this radius can be compared to the tidal radius of $r \sim 1.7$ estimated at perigalacticon from equation (11) of Oh, Lin & Aarseth (1995) (see also King 1962). The particles that have been stripped off from the main body produce a noticeable bend at $r \sim 4$, and continue outward into tidal tails. In addition, this figure indicates that the tidal forces exerted by the host galaxy during the formation of the first pair of tidal arms deform considerably the outer density profile of the main body, while the subsequent tidal forces have less impact on the outer density profile, so that it changes gradually with time. However, the particles included in each pair of tidal arms are nearly the same in number, regardless of the strength of the tidal forces, as shown in Table 1.

4 DISCUSSION

As far as the formation of the first pair of tidal tails is concerned, our dwarf galaxy model shows an evolutionary sequence which is very similar to that in previous studies (Piatek & Pryor 1995; Dehnen et al. 2004; Capuzzo Dolcetta et al. 2005; Montuori et al. 2007), as presented in Figs 1 and 3(a). That is, the tidal interaction of the dwarf galaxy, starting from apogalacticon, with its host galaxy generates a pair of tidal arms at a position close to perigalacticon, and that pair becomes more pronounced at the subsequent

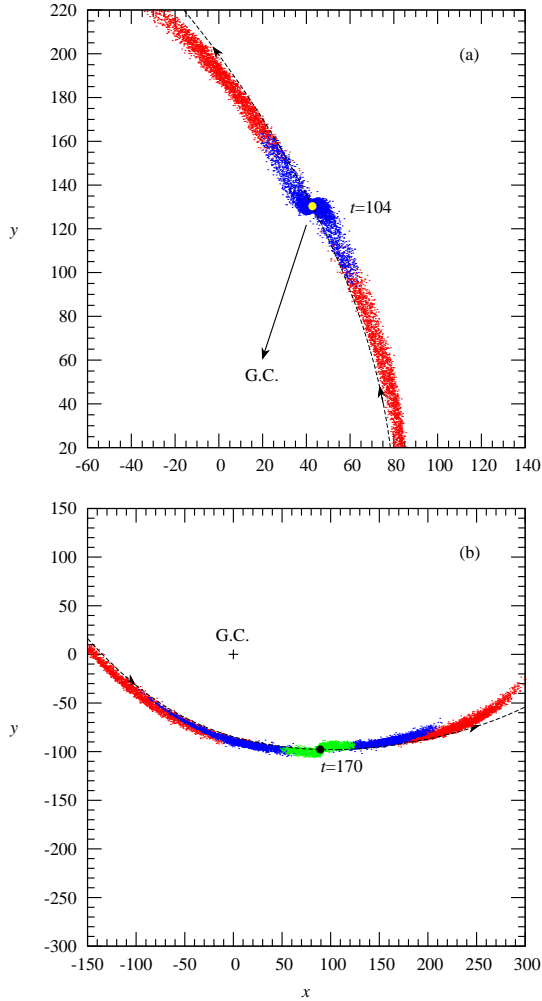


Figure 8. Two pairs of leading and trailing tidal arms at $t = 104$ (a), and three pairs of those at $t = 170$ (b), somewhat after pericentre passage projected on to the orbital plane. The red, blue, and green dots represent the particles constituting the first, second, and third formed arms, respectively. Only the arm particles are plotted. The dashed lines show the orbital path of the dwarf galaxy, while the arrows on them denote the directions of the orbital motion of the dwarf galaxy. The filled yellow and black circles indicate the positions of the centre of the dwarf galaxy at $t = 104$ and 170 , respectively. The long arrow with the label G.C. in (a) points to the centre of the host galaxy, while the + symbol in (b) shows the centre of the host galaxy. The tidal tails are represented on real scales.

apogalacticon. As explained qualitatively by Dehnen et al. (2004) on the basis of a simple analytic argument on orbital energy, one half of the pair contains particles which lose energy as a whole and move on to orbits slightly inside the orbital path of the main body of the dwarf galaxy, while the other half contains those which gain energy by and large and move on to orbits slightly outside that orbital path. Consequently, the former and latter particles constitute a leading and trailing tail, respectively. In fact, we have demonstrated in Fig. 4 that on average, leading-arm particles lose energy, while trailing-arm particles gain energy, when a pair of tidal arms is formed.

On the other hand, we have also shown in Fig. 4 that on the whole, leading-arm particles lose angular momentum,

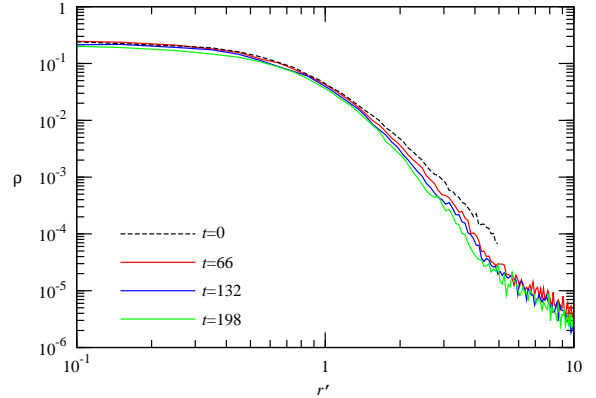


Figure 9. Spherically averaged density distributions of the main body of the dwarf galaxy around apogalacticons. Note that the initial model was truncated at $r' = 5$.

Table 1. Number of particles, N , and total mass fraction included in each tidal arm for the first three pairs of tidal tails. Here, the fraction is the ratio of the number of arm particles to that of the bound particles of the dwarf galaxy. The letters L and T denote leading and trailing arms, respectively.

	First arms		Second arms		Third arms	
	L	T	L	T	L	T
N	2705	2763	2790	2682	1914	2240
Per cent	5.41	5.53	6.27	6.02	4.90	5.73

while trailing-arm particles gain angular momentum. After the arm particles that have lost or gained angular momentum pass through their first apogalacticon, they lose or gain only a small amount of angular momentum subsequently. As the dwarf galaxy moves from an apogalacticon to the next perigalacticon, the distances from the arm particles to the centre of the host galaxy diminish, and owing to that approximate conservation of angular momentum, the velocities of leading-arm particles are increased while those of trailing-arm particles are decreased relative to the velocity of the centre of the dwarf galaxy. Consequently, near the perigalacticon the leading arm extends forward while the trailing arm elongates backward with respect to the main body of the dwarf galaxy. Therefore, as is demonstrated in Figs 3 and 8, the direction of the tidal arms becomes almost parallel to the orbital path of the dwarf galaxy around pericentre passage, which is often reported in the literature (Dehnen et al. 2004; Capuzzo Dolcetta et al. 2005; Montuori et al. 2007) without physical explanations. Subsequently, the arm lengths are decreased from the perigalacticon to the next apogalacticon again on account of that approximate conservation of angular momentum.

Regarding the formation mechanism of multiple tidal arms, we can see from Figs 2 and 3 that each pair of tidal arms never bifurcates with time, and that a fresh pair of tidal arms develops every time the dwarf galaxy moves from a perigalacticon to the next apogalacticon. It thus follows that the multiple pairs of tidal arms are generated by the repeated episode of tidal arm formation. However, even though a pair of tidal arms is formed repeatedly again and again,

the multiplicity itself cannot be recognized unless the angle between two pairs of tidal arms is different to some degree. Since the dynamical time of the dwarf galaxy is shorter than its orbital period, it recovers dynamical equilibrium soon after a pair of tidal arms is extracted at perigalacticon. Moreover, the gravitational effects of tidal arms are negligible, so that existing tidal arms do not affect the subsequent formation of tidal arms. Hence, the configuration of a forming pair of tidal arms with respect to the dwarf galaxy is determined only by its orbital phase. Now that the dwarf galaxy is moving on an eccentric Rosetta orbit that is not closed, the precession of the orbit results in a rotation of the orientation of newly forming arms extracted around perigalacticon, leading to differences in the position angles of these arm particles. The resulting multiplicity is recognizable at the apogalacticon where the extracted arms are well developed. In this way, the multiplicity of tidal arms is perceived. In fact, Fig. 7 proves that the secondly formed pair of tidal arms can be superposed on the first formed pair by rotating the angle between the two apogalacticons at $t \sim 132$ and ~ 198 , and that likewise, the thirdly formed pair can be fit with the secondly formed pair by rotating the angle between the two apogalacticons at $t \sim 198$ and ~ 264 . These angles rotated to superpose the density profiles of tidal tails correspond to the precessing angle resulting from the eccentric orbit of the dwarf galaxy. We thus find that multiple tidal arms are the outcome of repeated tidal arm formation amid the precessing motion. Although Montuori et al. (2007) described the formation of multiple tidal tails around GCs on the basis of the Coriolis acceleration term in their equation (5), they only pointed out the directions of tidal tails near the apo- and peri-galactic centres, and they never referred to the precession angle of the orbit.

In our experiment, the number of particles included in each pair of tidal arms is nearly identical for the first three pairs of tidal arms as found from Table 1. These particles produce similar density distributions at similar orbital positions for the three pairs of tidal arms (see Fig. 7). In addition, Fig. 5 reveals the similarity in the energy and angular momentum distributions of these three pairs. Therefore, each episode of tidal arm formation is independent of the previous episode(s). Again, this fact ensures that the phase of the tidal arm formation is specified only by the phase of the orbit of the dwarf galaxy.

We should discuss the detectability of multiple tidal tails. First of all, although dwarf galaxies are considered to be dark matter dominated (Mateo 1998; Gilmore et al. 2007), we have neglected a contribution of dark matter to our dwarf galaxy model. In such circumstances, it is conceivable that multiple tidal tails are predominantly made of dark matter. How much luminous matter is contained in tidal tails can be estimated from its total fraction outside the tidal radius of a progenitor dwarf galaxy. Probably, multiple tidal tails containing stars could also form for plausible models of dwarf galaxies despite the fact that they are dominated by dark matter. For example, according to the simulations of Lokas et al. (2013) in which the properties of tidal tails around dwarf galaxies orbiting a Milky Way-like host have been studied, both stellar and dark matter components develop tidal tails. On the other hand, as shown by Peñarrubia, Navarro & McConnachie (2008) and by Smith et al. (2013), dwarf galaxy models consisting of

stellar and dark matter components lose more than 90 per cent of the dark halo before affecting the stellar component. In this way, even if the stars are not self-gravitating, they reside in the innermost parts of the dark halo. Consequently, our one-component model for dwarf galaxies can still provide some insight into the physics for tidal tail formation and the multiplicity in general, and can serve as a basis for more complex multicomponent models. Next, obviously, we can observe the multiplicity more easily when the orbital plane of a dwarf galaxy is viewed from the direction to the line of sight as perpendicularly as possible. However, even though we are then placed at a preferred configuration with respect to the orbital plane, Fig. 8 indicates that near perigalacticon, tidal arms generated in subsequent episodes form a single coherent structure, which makes it difficult to distinguish each pair of them. As found from Figs 2 and 3, the situation is better around apogalacticon where at least trailing arms are spatially separated, providing information, in some cases, about the number of orbital rotations completed by the satellite. Thus, it is significant to discover those dwarf satellite galaxies presenting multiple tidal arms which lie around apogalacticon and whose orbital plane is nearly perpendicular to the line of sight.

As we have described in Section 1, our present analysis is applicable to GCs, although we do not include in our study the effects of disc shocking that would be expected for most of GCs. Therefore, it is likely that multiple tidal tails around GCs can be detected. Interestingly, NGC 288 has been reported to have multiple tidal tails (Leon et al. 2000). However, GCs are considerably less massive than dwarf galaxies, and so, long tidal tails, in general, would become sufficiently faint. In addition, since GCs are collisional systems in which mass segregation progresses, tidal tails consist primarily of less massive and less luminous stars as shown by Combes, Leon & Meylan (1999). Consequently, it might be more difficult to detect multiple tidal tails around GCs, even if they actually exist, than those around dwarf galaxies. As another view, GCs moving on highly eccentric orbits that are suitable for developing multiple tidal tails might have been selectively disrupted on the ground that they populate in the inner regions of our Galaxy where tidal effects are relatively strong.

5 CONCLUSIONS

We have examined how tidal tails are formed and evolve to generate multiple tidal features around a dwarf satellite galaxy moving on a highly eccentric orbit in a fixed potential of its host galaxy in which a disc component is neglected, assuming that the dwarf galaxy is a one-component system. We find that a pair of tidal tails is excited every time the dwarf galaxy passes through perigalacticon where it suffers strong tidal forces from the host galaxy, and that the extracted pair is added to the existing pair(s) of tidal tails, which leads to the multiplicity. We also find that the angle between two consecutively formed pairs of tidal tails is equal to the one arising from the precessing motion of the dwarf galaxy, when viewed on the orbital plane. This process should be valid for any satellite, regardless of whether it is a GC or a satellite galaxy. Whenever the satellite is on an eccentric orbit, the repeating tidal tail formation process at

perigalacticon, coupled with the precessing motion, should create multiple tidal tails.

In addition, we have demonstrated that especially for the first three consecutively formed pairs of tidal tails each pair shows, in effect, identical energy and angular momentum distributions as well as density distribution to one another. This fact indicates that each pair of tidal tails is formed almost independently of the pre-existing pair(s). It thus turns out that the phase of the tidal tail formation is specified basically by the phase of the eccentric orbit of a satellite system.

ACKNOWLEDGMENTS

We are grateful to Drs Andrew Benson, Michael Hilker, Andreas Koch, and Mike Rich for critical reading and valuable comments on the manuscript. We are also grateful to Drs Masaki Iwasawa and Keigo Nitadori for fruitful discussions on the angular momentum changes of arm particles. We are indebted to the anonymous referee for the valuable comments that have helped to improve the manuscript. SH thanks the hospitality of the Max-Planck Institut für Astronomie in Heidelberg where this research began and part of it was completed. AB acknowledges support from the Cluster of Excellence ‘Origin and Structure of the Universe’.

REFERENCES

- Balbinot E., Santiago B. X., da Costa L. N., Makler M., Maia M. A. G., 2011, *MNRAS*, 416, 393
 Barnes J., Hut P., 1986, *Nature*, 324, 446
 Belokurov V., Evans N. W., Irwin M. J., Hewett P. C., Wilkinson M. I., 2006, *ApJ*, 637, L29
 Binney J., 2008, *MNRAS*, 386, L47
 Boylan-Kolchin M., Springel V., White S. D. M., Jenkins A., 2010, *MNRAS*, 406, 896
 Capuzzo Dolcetta R., Di Matteo P., Miocchi P., 2005, *AJ*, 129, 1906
 Choi J.-H., Weinberg M. D., Katz N., 2007, *MNRAS*, 381, 987
 Coleman M. G., Da Costa G. S., Bland-Hawthorn J., Freeman K. C., 2005, *AJ*, 129, 1443
 Combes F., Leon S., Meylan G., 1999, *A&A*, 352, 149
 Dehnen W., Odenkirchen M., Grebel E. K., Rix H.-W., 2004, *AJ*, 127, 2753
 Diemand J., Kuhlen M., Madau P., 2007, *ApJ*, 667, 859
 Gilmore G., Wilkinson M. I., Wyse R. F. G., Kleyna J. T., Koch A., Evans N. W., Grebel E. K., 2007, *ApJ*, 663, 948
 Grillmair C. J., 1998, in Zaritsky D., ed., *ASP Conf. Ser. Vol. 136, Galactic Halos: A UC Santa Cruz Workshop*. Astron. Soc. Pac., San Francisco, p. 45
 Grillmair C. J., Johnson R., 2006, *ApJ*, 639, L17
 Grillmair C. J., Freeman K. C., Irwin M., Quinn P. J., 1995, *AJ*, 109, 2553
 Howley K. M., Geha M., Guhathakurta P., Montgomery R. M., Laughlin G., Johnston K. V., 2008, *ApJ*, 683, 722
 King I., 1962, *AJ*, 67, 471
 Klimentowski J., Lokas E. L., Kazantzidis S., Mayer L., Mamon G. A., Prada F., 2009, *MNRAS*, 400, 2162
 Koch A., Burkert A., Rich R. M., Collins M. L. M., Black C. S., Hilker M., Benson A. J., 2012, *ApJ*, 755, L13
 Küpper A. H. W., Lane R. R., Heggie D. C., 2012, *MNRAS*, 420, 2700
 Lee K. H., Lee H. M., Fahlman G. G., Lee M. G., 2003, *AJ*, 126, 815
 Lehmann I., Scholz, R.-D., 1997, *A&A*, 320, 776
 Leon S., Meylan G., Combes F., 2000, *A&A*, 359, 907
 Lokas E. L., Gajda G., Kazantzidis S., 2013, *MNRAS*, 433, 878
 Martínez-Delgado D., Alonso-García J., Aparicio A., Gómez-Flechoso M. A., 2001a, *ApJ*, 549, L63
 Martínez-Delgado D., Aparicio A., Gómez-Flechoso M. Á., Carrera R., 2001b, *ApJ*, 549, L199
 Martínez-Delgado D., Gómez-Flechoso, M. Á., Aparicio A., Carrera R., 2004, *ApJ*, 601, 242
 Martínez-Delgado D. et al., 2012, *ApJ*, 748, L24
 Mateo M., 1998, *ARA&A*, 36, 435
 Mateo M., Olszewski E. W., Morrison H. L., 1998, *ApJ*, 508, L55
 Montuori M., Capuzzo-Dolcetta R., Di Matteo P., Lepinette A., Miocchi P., 2007, *ApJ*, 659, 1212
 Muñoz R. R., et al., 2006, *ApJ*, 649, 201
 Odenkirchen M. et al., 2001, *ApJ*, 548, L165
 Odenkirchen M., Grebel E. K., Dehnen W., Rix H.-W., Cudworth K. M., 2002, *AJ*, 124, 1497
 Odenkirchen M. et al., 2003, *AJ*, 126, 2385
 Oh K. S., Lin D. N. C., Aarseth S. J., 1995, *ApJ*, 442, 142
 Peñarrubia J., Navarro J. F., McConnachie A. W., 2008, *ApJ*, 673, 226
 Peñarrubia J., Navarro J. F., McConnachie A. W., Martin N. F., 2009, *ApJ*, 698, 222
 Piatek S., Pryor C., 1995, *AJ*, 109, 1071
 Plummer H. C., 1911, *MNRAS*, 71, 460
 Press W. H., Flannery B. P., Teukolsky S. A., Vetterling, W. T., 1986, *Numerical Recipes: The Art of Scientific Computing*. Cambridge Univ. Press, Cambridge
 Rich R. M., Collins M. L. M., Black C. M., Longstaff F.A., Koch A., Benson A., Reitzel D. B., 2012, *Nature*, 482, 192
 Saviane I., Monaco L., Hallas T., 2010, in Bruzual G., Charlot S., eds, *Proc. IAU Symp. 262, Stellar Populations – Planning for the Next Decade*. Cambridge Univ. Press, Cambridge, p. 426
 Siegel M. H., Majewski S. R., Cudworth K. M., Takamiya M., 2001, *AJ*, 121, 935
 Smith R., Fellhauer M., Candlish G. N., Wojtak R., Fariás J. P., Blána M., 2013, *MNRAS*, 433, 2529
 Sofue Y., Rubin V., 2001, *ARA&A*, 39, 137
 Sohn S. T. et al., 2007, *ApJ*, 663, 960
 Sollima A., Martínez-Delgado D., Valls-Gabaud D., Peñarrubia J., 2011, *ApJ*, 726, 47
 Testa V., Zaggia S. R., Andreon S., Longo G., Scaramella R., Djorgovski S. G., de Carvalho R., 2000, *A&A*, 356, 127

APPENDIX A: ENERGY AND ANGULAR MOMENTUM CHANGES FOR TIDAL TAILS AT THE FORMATION EPOCH

Suppose that the tidal tails are extracted impulsively from the dwarf galaxy at pericentre. The energy change for the

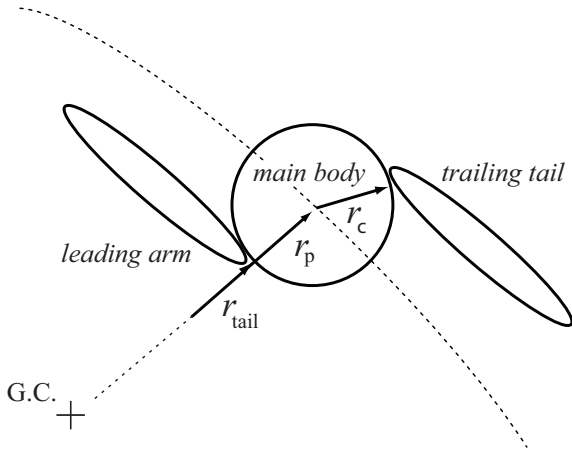


Figure A1. Schematic representation of the main body and the tidal tails, where r_p and r_c are the pericentre distance and the radius of the dwarf galaxy, respectively, and r_{tail} is a representative distance from the centre of the host galaxy to the leading or trailing tail.

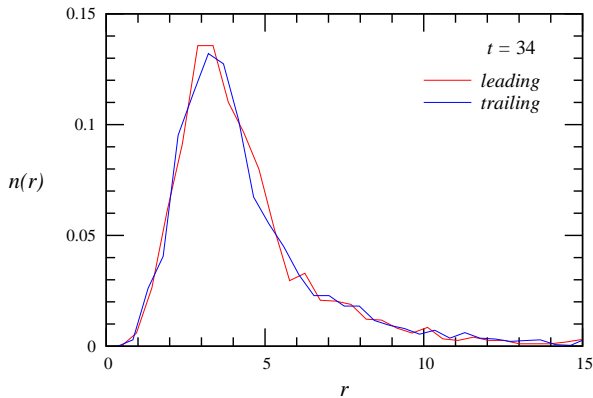


Figure A2. Fractional particle number distributions of the first formed tidal arms against the distance from the centre of the dwarf galaxy near the pericentre ($t = 34$).

arm particles arises from the difference in the host galaxy potential between the distances of the arm particles from the centre of the host galaxy before and after the extraction. From Fig. A1 in which the configuration of the main body and the tidal tails is illustrated, the value of this energy change can be estimated to be $\Delta E = \Phi(r_{\text{tail}}) - \Phi(r_p)$. Using equation (1), we obtain, in our dimensionless system of units, $\Delta E = v_c^2 \ln(r_{\text{tail}}/r_p) = v_c^2 \ln(1 \pm r_c/r_p) \sim \pm 18$, where the + and - signs correspond to the trailing and leading arms, respectively. In this calculation, we adopt the values of $v_c^2 = 282$, $r_c = 5$, and $r_p = 80$. Thus, ΔE agrees well with the amount of the energy lost by the leading arm, or that gained by the trailing arm, as shown in Fig. 4.

On the other hand, the angular momentum change for the arm particles is caused by stripping them off from the dwarf galaxy when it passes through the pericentre at the formation epoch ($t \sim 33$). Again, this stripping is supposed to be impulsive, so that the leading-arm particles will lose angular momentum, while the trailing-arm particles will gain angular momentum, by the amount of $\Delta L \sim v_p \Delta r$, where v_p and Δr denote, respectively, the orbital speed of

the main body at the pericentre, and the displacement between the centre of the main body and a representative position of each arm. In order to evaluate this representative position, we calculate the distances of the particles in the first pair of tidal arms from the centre of the dwarf galaxy. Fig. A2 shows the resulting fractional particle number distributions of this pair near the pericentre. We find from this figure that the typical value of Δr is $\sim \pm 3.5$, where the + and - signs correspond to the trailing and leading arms, respectively. At around the distance of $|\Delta r|$, the density bend can be found in Fig. 9, and so, this distance is considered to indicate the representative position for both arms. Consequently, we obtain $\Delta L \sim \pm 105$ using $v_p \sim 30$. This value of ΔL is close to the amount of the angular momentum lost by the leading arm, or that gained by the trailing arm, as shown in Fig. 4.

This paper has been typeset from a $\text{\TeX}/\text{\LaTeX}$ file prepared by the author.